3-D Numerical simulation of water flow over a broad-crested weir with openings

Article *in* ISH Journal of Hydraulic Engineering · March 2019

DOI: 10.1080/09715010.2019.1581098

ISH Journal of Hydraulic Engineering

ISSN: 0971-5010 (Print) 2164-3040 (Online) Journal homepage: https://www.tandfonline.com/loi/tish20

3-D Numerical simulation of water flow over a broad-crested weir with openings

Rasoul Daneshfaraz, Omar Minaei, John Abraham, Sorayya Dadashi & Amir Ghaderi

To cite this article: Rasoul Daneshfaraz, Omar Minaei, John Abraham, Sorayya Dadashi & Amir Ghaderi (2019): 3-D Numerical simulation of water flow over a broad-crested weir with openings, ISH Journal of Hydraulic Engineering, DOI: 10.1080/09715010.2019.1581098

To link to this article: https://doi.org/10.1080/09715010.2019.1581098

Published online: 01 Mar 2019.

ISH JOURNAL OF HYDRAULIC ENGINEERING
https://doi.org/10.1080/09715010.2019.1581098

Taylor & Francis
Taylor & Francis Group

3-D Numerical simulation of water flow over a broad-crested weir with openings

Rasoul Daneshfaraz[a], Omar Minaei[a], John Abraham[b], Sorayya Dadashi[a] and Amir Ghaderi[c]

[a]Department of Civil Engineering, Faculty of Engineering, University of Maragheh, Maragheh, Iran; [b]School of Engineering, University of St. Thomas, St Paul, MN, USA; [c]Department of Civil Engineering, Faculty of Engineering, University of Zanjan, Zanjan, Iran

ABSTRACT

The creation of an opening in a broad-crested weir body increases the discharge coefficient and reduces the water elevation behind the weir. In this study, three-dimensional numerical modeling is applied to investigate the water behavior, free-surface profiles, and velocity distributions over a broad-crested weir with one opening, two vertically arranged openings, and two horizontally arranged openings. The present study is limited to the above-described weir-opening arrangements. To determinate the most accurate turbulence model, results from the numerical simulation were compared with experimental data. Based on this comparison, the RNG turbulence model was chosen. The behavior of two horizontally arranged openings and the no-opening model were similar and critical flow occurred in two other models (one opening and two vertically arranged openings), downstream of the weir. Also, the maximum velocity in the models without openings was higher than in the other cases.

ARTICLE HISTORY
Received 29 March 2018
Accepted 7 February 2019

KEYWORDS
Numerical simulation; turbulence model validation; broad-crested weir; free-surface profiles; velocity distributions

1. Introduction

Due to the persistent and ubiquitous need for water for activities such as irrigation, human and animal consumption, manufacturing, and others, extensive efforts have been implemented world-wide for appropriate water management. One common water-management device is the weir which is used to modify the water-flow within rivers. Existing weirs are not typically responsive to water demand. Consequently, it would be advantageous if the water supply from these structures could be modified to meet fluctuating water demand. Therefore, new structures could replace existing structures or modifications could be made to current weirs to achieve this desired control. Candidate changes could include an extension of the weir crown or an opening up of the weir body to modify the flow. A large number of studies have been conducted of the flow over a broad-crested weir; some of them are discussed below.

Investigations of the flow over a curvilinear broad-crested weir indicates that the results of the renormalization – group κ–ε turbulence model (RNG) are closer to the experimental results than other models such as standard κ–ε model, the realizable κ–ε model, or the Shear Stress Transport κ–ω model (Simsek et al. 2016; Daneshfaraz and Ghaderi 2017; Daneshfaraz et al. 2017). Hoseini (2014) studied the flow pattern over a triangular broad-crested weir and he presented an empirical relation that can be used to calculate the discharge coefficient. Studies on broad-crested stepped spillways indicate that there is good agreement between experimental and numerical results. Also, the two–equation Renormalized Group (RNG) turbulence model has demonstrated an ability to predict flow over broad-created stepped spillways (Dolatshah et al. 2013). Experimental studies on embankment weirs with smooth and rough crests show that the discharge coefficient is reduced by increasing the crest roughness. Also, the upstream and downstream ramps did not have much effect on the discharge performance (Felder and Islam 2016).

A comparison of experimental results with CFD results indicates that both of these investigation methods are able to predict the water surface profiles for ogee and broad-crested weirs and their discharge coefficients (Haun et al. 2011; Daneshfaraz et al. 2014, 2016). The studies of mechanisms of the undular flow over the broad-crested weir suggests that the upstream face of the weir has a significant effect on the undular flow so that reducing the upstream face slope increases the relative wave length and decreases the relative wave height (Madadi et al. 2013). A vertical face downstream of a broad-crested weir can prevent cavitation at high discharge flow without having much effect on the discharge coefficient (Sargison and Percy 2009).

The discharge coefficients for embankment weirs are larger than the coefficients for weirs without upstream and downstream ramps (Azimi et al. 2012). The discharge coefficients for broad-crested weirs are related to the ratio of upstream Froude number to the downstream Froude number (F_u/F_d) and the oblique angle (Riha and Zachoval 2014). The solutions obtained using the κ–ε RNG model were obtained in significantly less time (approximately half) compared to solution time required for the standard κ-ε model (Ghazizadeh and Moghaddam 2016). The RNG model is able to predict free water surface flow in broad-crested weirs with similar performance to the Large-Eddy Simulation (LES) algorithm (Afshar and Hoseini 2013).

The maximum velocity near the bed of a broad-crested weir with three openings is less than that for a weir with one opening. Also, the hydraulic jump length downstream of the weir with three openings is less than the hydraulic jump length downstream of a weir with one opening (Saad and Fattouh 2016). Notably, the literature review highlights different types of hydraulic jumps and related behavior of energy dissipation (Sadeghfam et al. 2015). In a broad-crested weir with one opening where the opening is submerged, the upstream and downstream water depths are affected as well as the discharge flow (El-Belasy 2013). The hysteresis and bimodality behavior of

CONTACT Rasoul Daneshfaraz daneshfaraz@yahoo.com

hydraulic jump was investigated by Sadeghfam et al. (2017). Discharge coefficients improve when a pipe or opening runs along the bottom of the broad-crested weir (Abozeid et al. 2014).

A common problem with spillways is the accumulation of sediment in the reservoir. The creation of an opening in the spillway allows sediment to pass the opening and sedimentation decreases significantly. To the best knowledge of the authors, there are no existing studies that have been dedicated to this subject.

In this study, the authors investigate the flow behavior, free-surface profiles, and velocity distributions for broad-crested weirs with different hole configurations. For this purpose, three-dimensional numerical modeling was applied to flow over a broad-crested weir with one opening, with two vertically arranged openings, and with two horizontally arranged openings. Each of these configuration were studied with three side slopes (0.5H:1V, 1H:1V, 2H:1V).

2. The governing equations and the geometry models

2.1. The governing equations

The discharge of the weir is represented by the symbol Q_c and the discharge of the opening is symbolized by Q_o. The flow over a weir is calculated without considering any reduction of the coefficient of discharge (C_d) from Equation (1), (Henderson 1966):

$$Q_c = \frac{2}{3} B \sqrt{2g} H^{\frac{3}{2}} \tag{1}$$

Here, B represents the width of the weir, H is the upstream total head, and g is the gravitational acceleration term. Figure 1 shows the geometric parameters of the flow over the weir crest and the through the opening.

To calculate the discharge through the openings, available information from the literature was employed. Bodhaine (1968) examined flow through culverts and a discharge equation was written as:

$$Q_o = NA\sqrt{2g}\left(H + P - y - h_f\right)^{0.5} \tag{2}$$

where N is the number of openings in the weir, Q_o represents the discharge from the opening, A is the cross-sectional area of the opening, H is the total head above the crest, y is the water depth downstream of the opening, P is the weir height, and h_f is the energy lost as the fluid passes through the opening.

The total discharge over the crest weir and through the opening is calculated using Equation (3):

$$Q_{tot} = \sqrt{2g}\left(\frac{2}{3} B H^{1.5} + NA(H + P - y)^{1.5}\right) \tag{3}$$

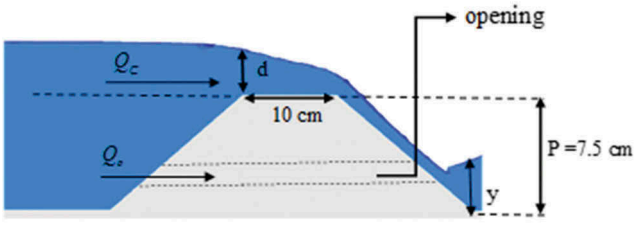

Figure 1. Schematic description of the physical situation.

2.2. Numerical simulation

The simulations were carried out using the Flow 3D software which is a CFD program for modeling multi-physics flow problems (Flow Science®, 2008). The software uses the Finite Volume Method to solve the three-dimensional Reynolds Averaged Navier–Stokes equations of fluid motion. These equations can be written in a Cartesian coordinate system (x, y, z) as follows:

$$V_F \frac{\partial \rho}{\partial t} + \frac{\partial(\rho u A_x)}{\partial x} + \frac{\partial(\rho v A_y)}{\partial y} + \frac{\partial(\rho w A_z)}{\partial z} = R_{SOR} \tag{4}$$

$$\frac{\partial u}{\partial t} + \frac{1}{V_F}\left(u A_x \frac{\partial u}{\partial x} + v A_y \frac{\partial u}{\partial y} + w A_z \frac{\partial u}{\partial z}\right) = -\frac{1}{\rho}\frac{\partial K}{\partial x} + G_x + f_x \tag{5}$$

$$\frac{\partial v}{\partial t} + \frac{1}{V_F}\left(u A_x \frac{\partial v}{\partial x} + v A_y \frac{\partial v}{\partial y} + w A_z \frac{\partial v}{\partial z}\right) = -\frac{1}{\rho}\frac{\partial K}{\partial y} + G_y + f_y \tag{6}$$

$$\frac{\partial w}{\partial t} + \frac{1}{V_F}(u A_x \frac{\partial w}{\partial x} + v A_y \frac{\partial w}{\partial y} + w A_z \frac{\partial w}{\partial z}) = -\frac{1}{\rho}\frac{\partial K}{\partial z} + G_z + f_z \tag{7}$$

These equations are expressed in terms of the (u,v,w) Cartesian velocity components. The A symbols are the fractional areas associated with the flow. The G terms are local accelerations of the fluid, and the f terms are related to frictional forces in the respective directions. The symbol ρ signifies the fluid density and K indicates local pressure.

Flow 3D includes popular turbulence models such as κ–ε, κ–ε RNG and large eddy simulation (LES). Modeling turbulent flow requires selecting a suitable turbulence model, which creates a closed form of the Navier–Stokes equations. In κ–ε Re-Normalization Group analysis (RNG), flow turbulence parameters are obtained through mathematical equations based on a stochastic technique. This method is particularly accurate for solving turbulent straining flows by having an additional term ε. This model is based on the standard κ–ε model developed by Jones and Launder (1972) and Launder and Spalding (1972). The modification was articulated by Yakhot et al. (1992). While its form is identical to that of the standard method, slight modifications are made in the fitted constants used in the turbulent transport equations.

The Flow 3D software uses the VOF technique to model the free surface flow and the FAVOR technique for modeling the rigid body and walls. This method is described as follows:

$$\frac{\partial F}{\partial t} + \frac{1}{V_f}\left(\frac{\partial}{\partial x}(F u A_x) + \frac{\partial}{\partial y}(F v A_y) + \frac{\partial}{\partial z}(F w A_z)\right) = 0 \tag{8}$$

in which F is the fraction function, F = 0 when a cell is empty with no water inside and F = 1 when the cell is fully water.

2.3. Model geometry

The required steps for numerical simulation of flow over the describe spillways are as follows: (1) create the geometry of

the flow domain; (2) create the computational mesh; (3) define all boundary and initial conditions; (4) complete the flow simulation; and (5) validate and interpret the results.

The upstream and downstream side slopes were identical and the simulation was performed for three different slope values (0.5H:1V 1H:1V 2H:1V). Each of these three models has four different geometries (no opening, a single opening, two horizontally aligned openings, and two vertically aligned openings). The input discharge was variable in the range of 0.0012–0.0032 m^3/s. The total number of simulations was 84.

The scale of models is taken from the Aksoy and Doğan (2016) experiment. The crest length, weir height, and channel width were identical in all models and were 0.075, 0.1, and 0.15 m, respectively. The area of the openings in all cases (one opening and two openings) was 6 square centimeters. Consequently, opening diameters for the one opening and two opening cases were 0.0276 and 0.0195 m, respectively. To control the flow downstream, a sill with the side slope 2H:1V was placed at the end of channels. Figure 2 shows schematics and geometry of models.

2.4. Computational grid and boundary conditions

Various models were tested to choose a suitable mesh. According to the performed sensitivity mesh analysis (Table 1) and comparing the water surface profile obtained from numerical solution with experimental results, three different mesh sizes are used.

The flow domain was discretized by 832,050 cubic mesh elements. A symmetry boundary condition is applied to the top boundary. A volumetric flowrate that ranged from 0.0012 to 0.0032 m^3/s was applied to input flow. An outflow boundary condition was applied to the downstream boundary. Finally, wall boundary conditions were defined for walls and the channel bed which acts as a no-slip surface. The grid mesh lines and boundary conditions imposed on the models are shown in Table 2 and Figure 3

3. Discussion and analysis

3.1. Comparison between experimental results and numerical solutions

The water surface profile from the present numerical analysis was compared with the experimental data from Aksoy and Doğan (2016). In order to find the best turbulence model for three different discharge rates (0.0032, 0.0020, 0.0012 m^3/s) with three Reynolds numbers (27, 18, 12×10^4), calculations were performed using three turbulence models κ–ε RNG, κ–ε, and LES. Then profiles of the three turbulence models were compared with experimental results. The 3D water surface and flow lines for the three turbulence models are shown in Figures 4 and 5. Results show that the LES turbulence model is in better agreement with experiments than the other two models; however, the other two models downstream water levels are smooth while in the LES model, the water surface exhibits an undular flow. Such an undular flow was not observed in the experiments. The LES turbulence model is often used for predicting the flow with high levels of turbulence and the simulation filters turbulence by spatial scale, modeling scales that are smaller than the local grid size. In this study, since the turbulence structures are large, the LES turbulence model was not used for further simulation. First, LES is very computationally expensive and it led to unphysical surface-flow behavior.

Velocity vectors and flow lines after the weir in the LES model are necessarily unsteady and do not reflect a time-averaged flow field. On the other hand, for the RANS-based

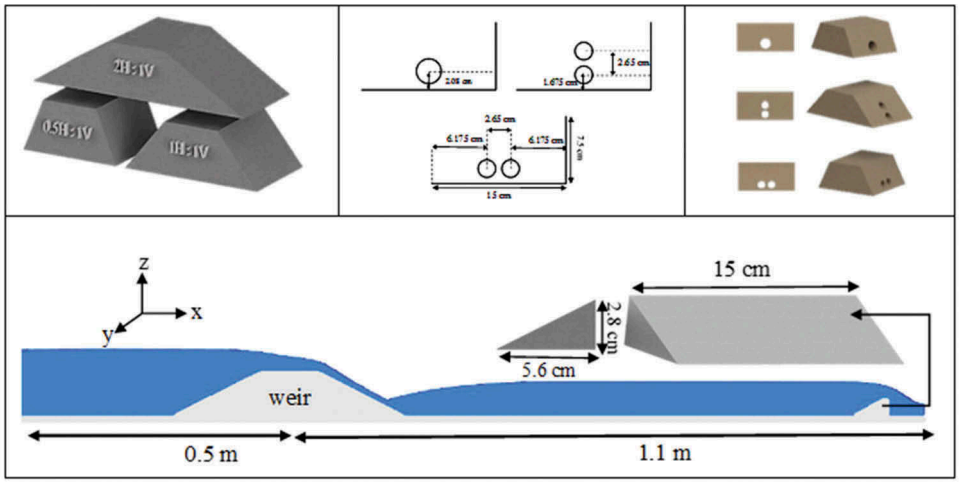

Figure 2. Schematic diagrams of the models, including the weir, circular openings, and side views.

Table 1. Mesh sensitivity analysis.

Test no.	Total number of cells	Max aspect ratio	Discharge (m^3/s)	RMSE[a] (cm) $\sqrt{\frac{1}{n}\sum_{1}^{n}(X_{exp}-X_{num})^2}$	MAPE[b] (%) $100 \times \frac{1}{n}\sum_{1}^{n}\left\|\frac{X_{exp}-X_{num}}{X_{exp}}\right\|$
T1	421,494	1	0.0012	1.512	24.43
T2	574,126	1	0.0012	1.128	19.74
T3	832,050	1	0.0012	0.751	12.11

[a]Root Mean Square Error (RMSE), X_{exp}: Experimental value of X, X_{num}: Numerical value of X, n: Count of data.
[b]Mean Absolute Percentage Error (MAPE), X_{exp}: Experimental value of X, X_{num}: Numerical value of X, n: Count of data.

Table 2. Applied boundary conditions.

Software	Upstream boundary	Downstream boundary	Free surface boundary	Floor boundary	Lateral boundaries
FLOW-3D	Volume flow rate	Outflow	Symmetry	Wall	Wall

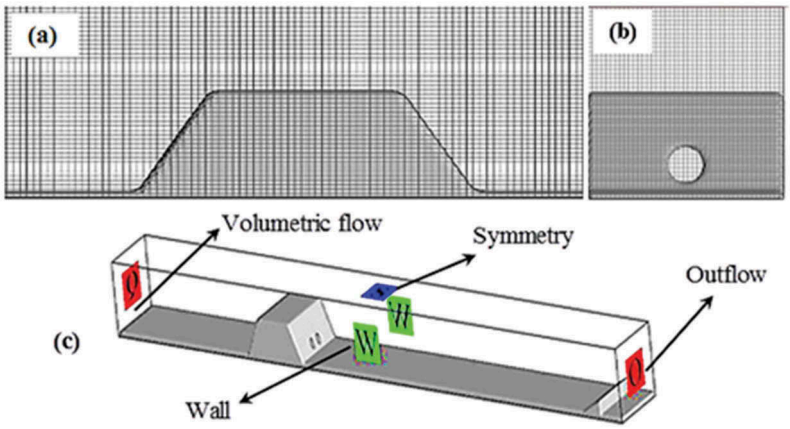

Figure 3. Computer image of the broad-crested weir and computational mesh (a) side view, (b) cross sectional view, (c) boundary condition annotations.

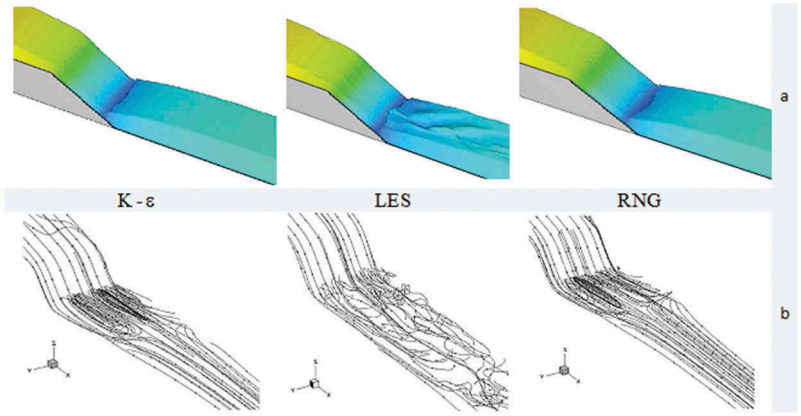

Figure 4. Comparison of free water surface levels for different turbulence models (a) surface elevation, (b) streamlines.

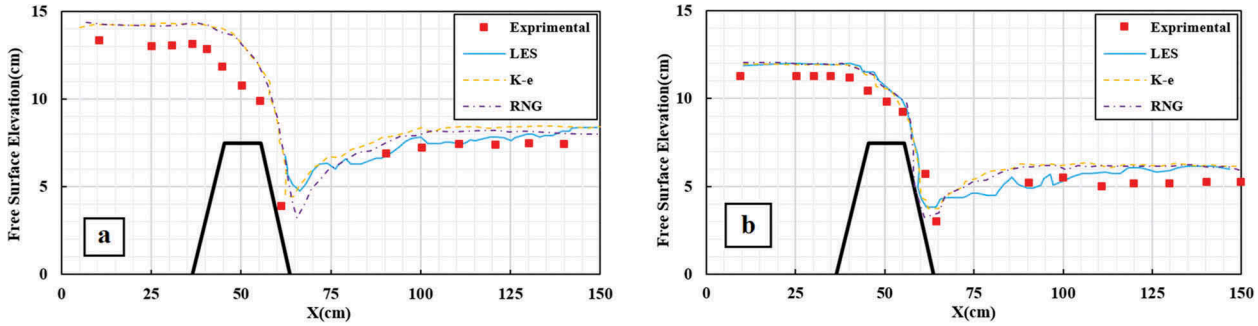

Figure 5. Comparison of free water surface profiles, experimental data from (Aksoy and Doğan (2016)) model parameters, 1H:1V; (a) Q = 0.0032 m^3/s, (b) Q = 0.002 m^3/s.

models, the downstream flow is time-averaged (time-averaged results are sufficient for the present comparison). For these reasons, the RANS results will be pursued in more depth.

For the numerical/experimental comparison, statistical measures such as mean absolute error (MAE), mean absolute percentage error (MAPE), the correlation coefficient (R^2), and root-mean-square error (RMSE) were calculated. The statistical indices are listed in Table 3 for the weir without an opening with both upstream and downstream side slopes 1H:1V and for three different discharge rates.

The benefits of using RMSE and MAE indices are that the scale results of these errors is the unit scale of the experimental parameter and their ideal values are both zero. This means that the model whose value of this index is closer to zero represents the more accurate calculation. According to the results presented in Table 3, it is observed that the RNG and the κ-ε turbulence models have better correlation coefficients than the LES model. The performance of the κ–ε model on average is 20% is better than the RNG model.

Table 3. Statistical indices for three turbulent models and for three flow rates.

turbulence model	Discharge (m^3/s)	R^2	MAPE (%)	MAE (cm)	RMSE (cm)
κ–ε	0.0032	0.9908	14.88	1.141	1.172
	0.0020	0.9862	13.02	0.868	0.930
	0.0012	0.9864	12.16	0.681	0.751
RNG	0.0032	0.9869	13.46	1.036	1.112
	0.0020	0.9864	13.00	0.871	0.932
	0.0012	0.9863	12.13	0.681	0.751
LES	0.0032	0.9757	11.39	0.911	1.044
	0.0020	0.9880	10.51	0.704	0.755
	0.0012	0.9464	9.68	0.596	0.610

MAPE shows the difference between the experimental and numerical data; lower values signify a better agreement. By comparing MAPE for different models and three different flow rates, it was found that the LES model has a lower error (on average 10.53) compared to the other two turbulence models. The RNG turbulence model is more accurate than the κ–ε model. Comparison of statistical measures for different flow rates showed that as the discharge increases, the simulation errors increase and model performance decreases. Comparison between experimental data and the numerical simulation showed that RNG model gives more reasonable results than the other two models. Figure 6 shows comparisons between the water surface profiles for these three turbulence models with experimental data and with flow rates of 0.002 and 0.0032 m^3/s.

It is observed that for a flow rate of 0.0032 m^3/s, the flow profiles differ more significantly from the experimental results upstream of the weir. Comparing the flow profiles simulated by the three turbulence models upstream of the weir and on the weir crest indicates that the simulated results are in excellent agreement with each other. Downstream, the surface profile calculated by the LES model shows a waveform. The intensity of this wave decreases with distance in the hydraulic jump area. In this turbulence model, the downstream flow is irregular. At low flow rates, the RNG and κ–ε simulations are in very good agreement. Increases to the discharge flow with the RNG turbulence model provide better performance, and in this study, this model is used for subsequent calculations.

3.2. Water flow profile

A comparison of the free surface profiles along the stream width shows that there is very little difference between them (Figure 6). For the no-opening cases, the flow depth was quite uniform along the channel width. It is expected that the free surface profiles would be different for models with openings, particularly near the location of holes. The two vertically aligned holes exhibit a profile that is greater than for the other cases. At the weir crest, the free water surface profiles were very consistent.

For all models, in the region upstream of the weir, the flow regime was subcritical; critical flow was formed on the weir crest. On the downstream side of the weir, the flow accelerates and becomes supercritical. At the end of the weir crest, negative pressure locations form locally. Figure 7 show streamlines upstream, downstream, and through openings for 0.5H:1V geometries with a 0.002 m^3/s discharge. Generally, flow lines in all models were parallel upstream and flow was laminar upstream of the weir with the flow lines displaying some curvature close to the weir.

In models with no openings, the flow curvature starts gradually before reaching the weir body and in the weir, streamline density (and flow velocity) is greatly increased. For the cases with an opening, the upstream flow approaches the weir and then subdivides into two or three portions according to the number of openings. Here again, the flow accelerates as it passes over the weir or through the openings, but the acceleration is less than that for the no-opening case. This finding is expected. Downstream of the weir, all cases display some degree of flow disturbance which is characterized by a recirculation zone at the free surface. The no-opening case leads to a more compact and vigorous recirculation zone whereas the other cases present an elongated but less intense zone.

The free water surface profiles (one opening, two horizontal openings and two vertical openings) overlap and only at the toe of the weir was there a small difference between them. The jump length increases with increasing discharge. The critical depth was formed on the downstream side of the weir crest and it extends further downstream with increasing discharge. For a discharge of 0.0016 m^3/s, the locations of the critical depth formation for models with one opening, two vertical openings, and two horizontal openings were 0.532, 0.535, and 0.5 m, respectively. For a discharge of 0.0032 m^3/s, the results were 0.535, 0.549, and 0.508 m, respectively. Comparison of water elevation for models with and without openings is provided in Figure 8.

During the transformation from subcritical to supercritical flow, a critical flow is formed on the weir crest. The critical

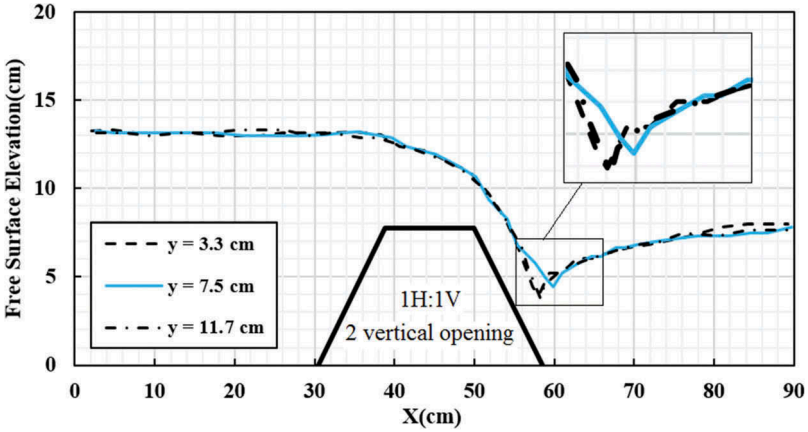

Figure 6. Comparison of the free-water surface in the channel width direction, (Q = 0.002 m^3/s), RNG turbulence model used.

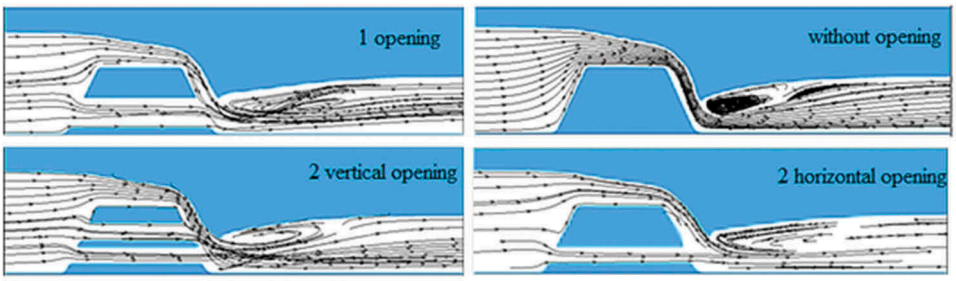

Figure 7. Flow lines over and through the weir for a 0H:1V model, RNG turbulence model used.

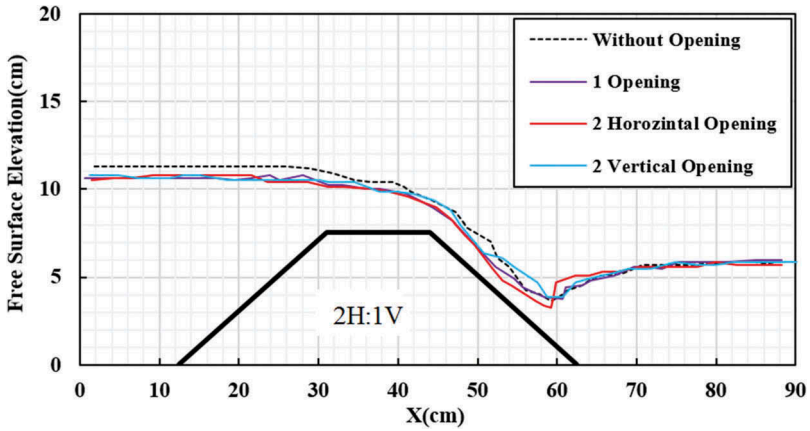

Figure 8. Comparison of free surface water flow for the with- and without-opening cases, discharge rate 0.002 m^3/s.

depths along the weir crest for different configurations are shown in Figure 9.

The critical depth is formed in the middle of the weir crest x = 0.5 m for the no opening cases and for the two horizontal opening cases. In models with an opening or with two vertical openings, the critical depth was directed toward the downstream side. Also, the critical depth in these two cases is greater than the no opening and two horizontal openings cases. In the two vertical openings model, the location of critical depth was shifted downstream by increasing the side slope.

3.3. Velocity distributions

The velocity distributions are extracted from several points along the crest and downstream of the weir. First, a comparison between the velocity distribution profiles on the weir crest for four different geometry patterns was conducted, as displayed in Figure 10.

Figure 10 shows that in models without openings, the velocity is considerably higher than cases with openings. In the cases with openings, some of the flow passes through the opening and the rest of the flow passes over the weir crest. This reduces the overpassing velocity compared to the no-opening case. Also, as displayed in Figure 11, the flow depth in the cases with openings has a decreased depth of weir crest flow.

Next, Figure 12 shows that downstream of the weir, there is a change in the flow velocity direction due to the vortex flows in the hydraulic jump region. Comparison of the velocity profiles in this region for different models shows that in cases with opening(s), the maximum velocity occurs at a greater depth and the velocity maximum is less than for cases without any openings. Downstream of the weir there are two masses of flow, one flowing from the crest and the other passing through the opening area and having different directions. This confluence causes the total velocity to decrease where the flow streams collide. The results for the 2H:1V model with a discharge of 0.0014 m^3/s shows that at the low flow rates, the overflow velocity was larger and was calculated to be 1.38 m/s for overflow weir and 1.25 m/s for the weir.

The velocity profiles for different weirs with and without openings are shown in Figure 13. The flow through the

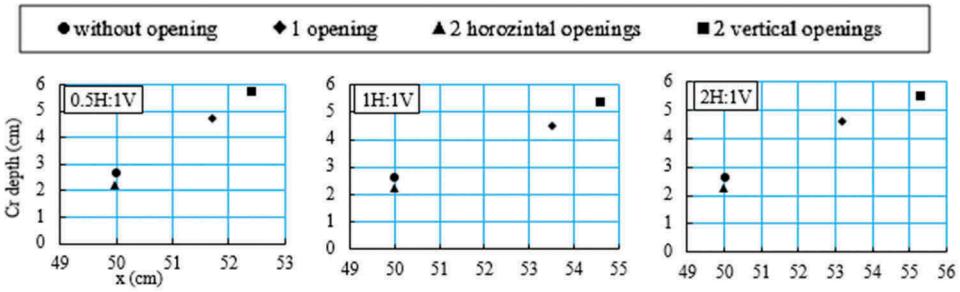

Figure 9. Critical depth over weir crest in deferent models.

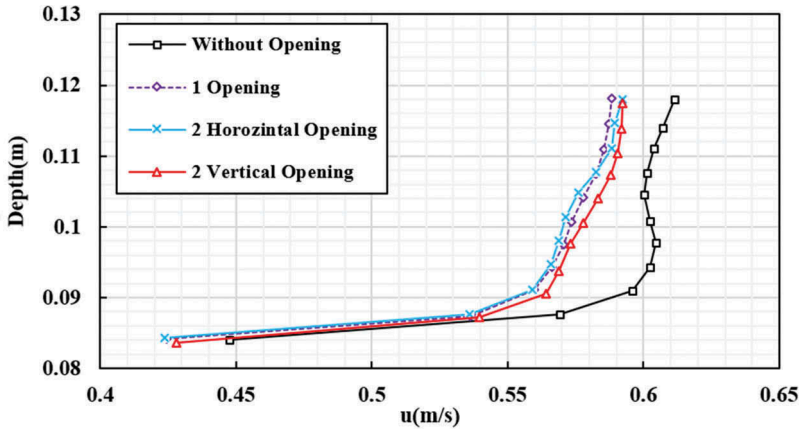

Figure 10. Velocity distributions for different models in the weir crest (2H:1V, x = 0.5 m, y = 0.075 m, Q = 0.0032 m^3/s) Velocity distributions for different models in the weir crest (2H:1V, x = 0.5 m, y = 0.075 m, Q = 0.0032 m^3/s).

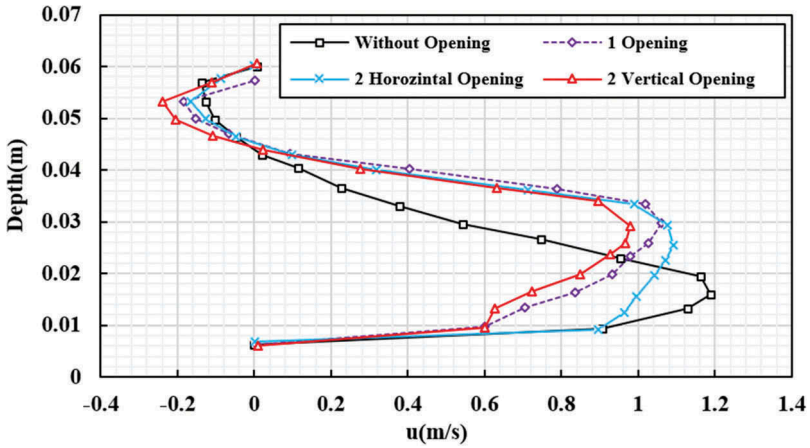

Figure 11. Velocity distributions for different models in downstream of weir crest (2H:1V, x = 0.5 m, y = 0.075 m, Q = 0.0032 m^3/s) Velocity distributions for different models in downstream of weir crest (2H:1V, x = 0.5 m, y = 0.075 m, Q = 0.0032 m^3/s).

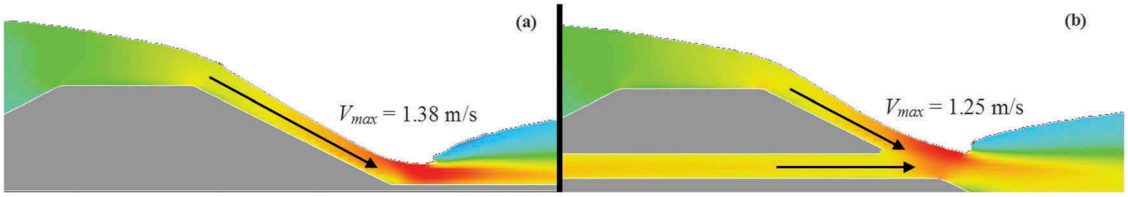

Figure 12. How to reach the flow downstream of the weir for (a) without opening, (b) having an opening. (2H:1V, Q = 0.0032 m^3/s) How to reach the flow downstream of the weir for How to reach the flow downstream of the weir for (a) without opening, (b) having an opening. (2H:1V, Q = 0.0032 m^3/s).

opening is seen to completely fill the channel and the velocity is largest at the center and near the opening. It is generally observed that the velocity inside the openings is greater than the velocity at the weir crest. This causes the maximum fluid velocity to be downstream of the overflow.

4. Conclusion

In this study, the flow through a broad-crested weir with and without openings and with different slopes was investigated using numerical simulation. It is noteworthy that there are limited studies that have investigated the flow behavior through these types of spillways. The simulations were conducted for four configurations (without any openings, 1 opening, 2 horizontally, and 2 vertically arranged openings). Each of these models was simulated for three different slopes (0.5H:1V, 1H:1V, 2H:1V). The range of discharge varied from 0.0012 to 0.0032 m^3/s. In order to verify the numerical results and select the most appropriate turbulence model, the CFD results were compared with the experimental results. The following list is a summary of the results:

(1) The accuracy of LES turbulence model was lower than the κ–ε RNG and standard κ–ε models. In the simulation carried out using the LES model, the free surface profiles downstream of the weir was undular while in the other two models it was smooth. The κ–ε RNG turbulence model, however, outperformed the standard κ–ε model.
(2) By increasing the flow rate, the agreement between the turbulent simulations and experiments improved. Comparison of the models showed that the simulation results were well correlated with the experimental data.
(3) In models with an opening, the streamlines inside the reservoir were gradually curved as the fluid

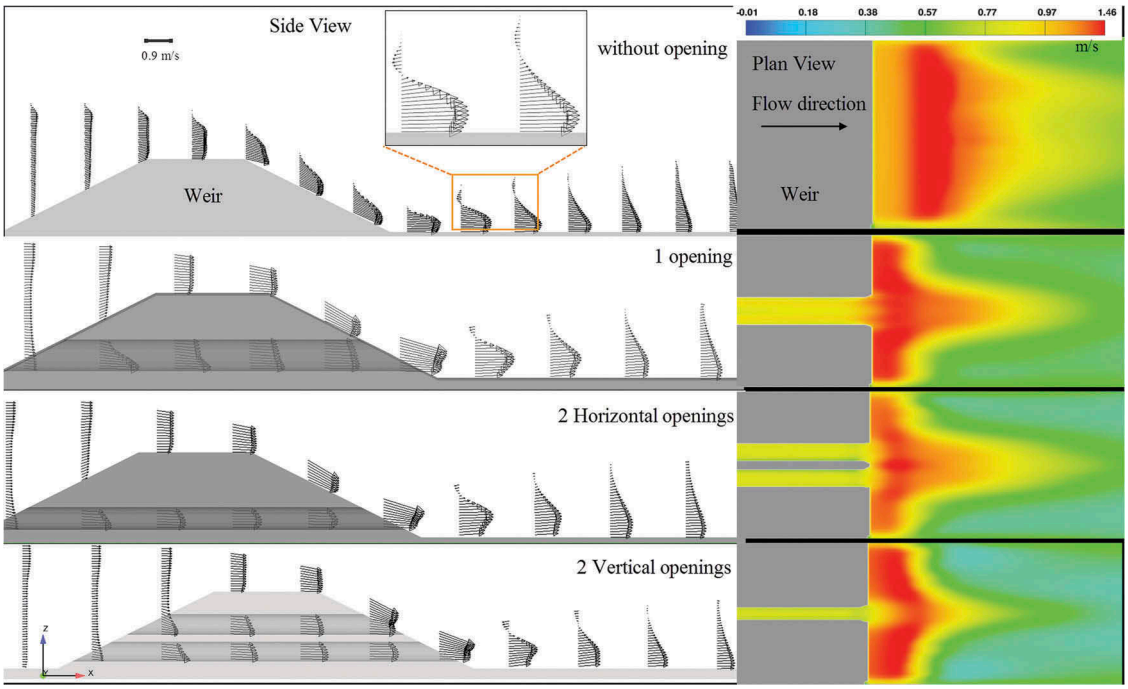

Figure 13. Velocity distribution profiles for models with and without opening(s). (2H:1V, Q = 3177 cm^3/s).

approached the weir. The flow divides into two or more parts when it approaches the weir; the upper part overflows the crest and the lower part passes through the opening(s).

(4) The velocity of flow passing through the openings is greater than the velocity over the weir crest.
(5) The flow profiles were overlapping for all three types of openings and there is only a small difference at the toe of the weir. The upstream head is decreased by including an opening in the weir body.
(6) The free surface profiles were different for the three side slopes in the downstream and hydraulic jump areas and in the other points those were overlapping.
(7) The behaviors of two horizontal openings and the no-opening model were similar and the critical flow occurred in two other models (one opening and two vertical openings), in the near downstream locations.
(8) Further studies can focus numerically and experimentally on the wide configurations of spillway and discharge rate.

Disclosure statement

No potential conflict of interest was reported by the authors.

References

Abozeid, G., El-Belasy, A.M., and Shehata, S.M. (2014). "Simulation of flow over weirs with bottom pipes (Case study: Bahar Hasan Wasef Weir)." *J. Eng. Sci.*, 42(14), 891–904.

Afshar, H., and Hoseini, S.H. (2013). "Experimental and 3-D numerical simulation of flow over a rectangular broad-crested weir." *Int. J. Eng. Adv. Technol.*, 2(6), 2249–8958.

Aksoy, A.O., and Doğan, M. (2016). "Experimental investigation of the approach angel effects on the discharge efficiency for broad crested weirs." *Anadolu Univ. J. Sci. Technol-A. Appl. Sci. Eng.*, 17(2), 279–286. doi:10.18038/btda.48930

Azimi, A.H., Rajaratnam, N., and Zhu, D.Z. (2012). "Discharge characteristics of weirs of finite crest length with upstream and downstream ramps." *J. Irrig. Drain. Eng.* doi:10.1061/(ASCE)HY.1943-7900.0001110

Bodhaine, G.L. (1968). *Measurement of peak discharge at culverts by indirect methods*, United States, Geological Survey.

Daneshfaraz, R., and Ghaderi, A. (2017). "Numerical investigation of inverse curvature ogee spillway." *Civil Eng. J.*, 3(11), 1146–1156. doi:10.28991/cej-030944

Daneshfaraz, R., Joudi, A.R., Ghahramanzadeh, A., and Ghaderi, A. (2016). "Investigation of flow pressure distribution over a stepped spillway." *Adv. Appl. Fluid Mech.*, 19(4), 811. doi:10.17654/FM019040811

Daneshfaraz, R., Kaya, B., Sadeghfam, S., and Sadeghi, H. (2014). "Simulation of flow over ogee and stepped spillways and comparison of finite volume and finite element methods." *J. Water Res. Hydraul. Eng.*, 3(2), 37–47.

Daneshfaraz, R., Sadeghfam, S., and Ghahramanzadeh, A. (2017). "Three-dimensional numerical investigation of flow through screens as energy dissipators." *Can. J. Civil Eng.*, 44(10), 850–859. doi:10.1139/cjce-2017-0273

Dolatshah, A., Shokouhi, S.S., Vosoughifar, H.R., and Rahnavard, Y. (2013). "Evaluation type of flow regime over broad-crested stepped spillways using a hybrid FVM-ANN approach." *J. World Environ. Water Resour. Congr.*, 1709–1718. Showcasing the Future. doi:10.1061/9780784412947.168

El-Belasy, A.M. (2013). "Developing Formulae for combined weir and orifice (case study: EL-Fayoum weirs)." *Alex. Eng. J.*, 52(4), 763–768. doi:10.1016/j.aej.2013.08.001

Felder, S., and Islam, N. (2016). "Hydraulic performance of an embankment weir with rough crest." *J. Hydraul. Eng.*, 143(3), 04016086. doi:10.1061/(ASCE)HY.1943-7900.0001255

Flow Science. (2008). *Incorporated: FLOW-3D Users Manual. Version 9.3*. Flow Science, Inc., Santa Fe, New Mexico.

Ghazizadeh, F., and Moghaddam, M.A. (2016). "An experimental and numerical comparison of flow hydraulic parameters in circular crested weir using flow3D." *Civil Eng. J.*, 2(1), 23–37.

Haun, S., Olsen, N.R.B., and Feurich, R. (2011). "Numerical modeling of flow over trapezoidal broad-crested weir." *J. Eng. Appl. Comput. Fluid Mech.*, 5(3), 397–405. doi:10.1080/19942060.2011.11015381

Henderson, F.M. (1966). *Open-channel flow*, Macmillan, New York, 269–277.

Hoseini, S.H. (2014). "Experimental investigation of flow over a triangular broad-crested weir." *ISH J. Hydraul. Eng.*, 20(2), 230–237. doi:10.1080/09715010.2014.884359

Jones, W.P., and Launder, B.E. (1972). "The prediction of laminarization with a two-equation model of turbulence." *Int. J. Heat. Mass. Trans.*, 15, 301–314. doi:10.1016/0017-9310(72)90076-2

Launder, B.E., and Spalding, D.B. (1972). *Mathematical models of turbulence*, Academic Press, London.

Madadi, M.R., Dalir, A.H., and Farsadizadeh, D. (2013). "Control of undular weir flow by changing of weir geometry." *J. Flow. Meas. Instrum.*, 34, 160–167. doi:10.1016/j.flowmeasinst.2014.05.014

Riha, J., and Zachoval, Z. (2014). "Discharge coefficient of a trapezoidal broad-crested side weir for low approach Froude numbers." *J. Hydraul. Eng.*, 140(8), 06014013. doi:10.1061/(ASCE)HY.1943-7900.0000889

Saad, N.Y., and Fattouh, E.M. (2016). "Hydraulic characteristics of flow over weirs with circular openings." *Ain Shams. Eng. J.*, doi:10.1016/j.asej.2016.05.007

Sadeghfam, S., Akhtari, A.A., Daneshfaraz, R., and Tayfur, G. (2015). "Experimental investigation of screens as energy dissipaters in submerged hydraulic jump." *Turk. J. Eng. Environ. Sci.*, 38(2), 126–138. doi:10.3906/muh-1401-15

Sadeghfam, S., Khatibi, R., Hassanzadeh, Y., Daneshfaraz, R., and Ghorbani, M.A. (2017). "Forced hydraulic jumps described by classic hydraulic equations reproducing cusp catastrophe features." *Arabian J. Sci. Eng.*, 42(9), 4169–4179. doi:10.1007/s13369-017-2616-x

Sargison, J.E., and Percy, A. (2009). "Hydraulics of broad-crested weirs with varying side slopes." *J. Irrig. Drain. Eng.*, 135(1), 115–118. doi:10.1061/(ASCE)0733-9437(2009)135:1(115)

Simsek, O., Akoz, M.S., and Soydan, N.G. (2016). "Numerical validation of open channel flow over a curvilinear broad-crested weir." *Prog. Comput. Fluid Dyn. Int. J.*, 16(6), 364–378. doi:10.1504/PCFD.2016.080055

Yakhot, A., Orszag, S.A., Thangam, S., Gatski, T.B., and Speziale, C.G. (1992). "Development of turbulence models for shear flows by a double expansion technique." *Phys. Fluids*, 4, 1510–1520. doi:10.1063/1.858424